Operating Range Enhancement by Tip Leakage Vortex Breakdown Control of a Centrifugal Compressor

Isao Tomita[1] and Masato Furukawa[2]

[1] Research & Innovation Center, Mitsubishi Heavy Industries, Ltd.
5-171-1, Fukahori-Machi, Nagasaki, Japan
[2] Department of Mechanical Engineering, Faculty of Engineering, Kyushu University
744 Motooka, Nishi-ku, Fukuoka, Japan

ABSTRACT

Centrifugal compressor applied to turbochargers is required to operate stably in wide range from choking to surging. In our past research, it was suggested that impellers which induced tip leakage vortex breakdown at relatively high flow rate might stabilize internal flow by generating circumferential uniform blockage region near blade tip at low flow rate. In this study, authors investigated whether modifying a given impeller to induce the tip leakage vortex breakdown could reduce the surging flow rate or not.

Pressure measurement of the conventional impeller showed that unstable pressure fluctuation occurred at smaller flow rate side than the peak pressure point. Furthermore, it was clarified by unsteady numerical calculation that the rotating stall occurred with circumferentially non-uniform reverse flow. On the other hand, in the new impeller increasing its inducer loading, unsteady numerical calculation showed that the blade tip leakage flow was strengthened and generated a circumferentially uniform blockage region, which could stabilize its internal flow.

As a result of performance test of the new impeller, considering that the surging flow rate at the same shaft speed was reduced by 3% and the pressure ratio at the surging point had been improved from 2.8 to 2.9, the surging flow rate at the pressure ratio of 2.8 could be reduced by 8%. In this way, it was found that the tip leakage flow was dominant with the stall phenomenon of the centrifugal compressor, and it was also confirmed that the tip leakage vortex control was one of the effective means for the operation range enhancement.

NOMENCLATURE

BPF: Blade Passing Frequency
π: Total to Total Pressure Ratio
Q*: Normalized Air Flow Ratio
η*: Normalized Efficiency Ratio
H_n: Normalized Helicity
V_z: Axial Velocity

INTRODUCTION

Operating range enhancement of centrifugal compressor for turbochargers is strongly demanded as engine development upgrades. However, how to control internal flow structure to enhance the operating range has been hardly understood because strong secondary flow due to the centrifugal and Coriolis force causes extremely complicated flow fields in centrifugal compressor impellers especially at low flow rate condition. Therefore, phenomena near surging or stall condition have not been clarified as for the axial compressor.

Regarding to rotating stall of the axial compressor, Moore and Greitzer[1] [2] showed that the flow field in the compressor became unstable at the maximum pressure rise point based on the theoretical model of the compressor, and its model was confirmed experimentally by McDougall[3], Garnier[4], Day[5], Poensgen and Gallus[6]. It was shown that disturbance wave of small scale rotating stall cells had a scale about 2-3 times of blade pitch.

The structure model of the small scale rotating stall cell was proposed experimentally by Inoue[7] [8]. Its model was that tornado type vortex with a leg on its blade suction surface caused a new leading edge separation on next blade. Yamada et al.[9] confirmed by numerical analysis that the small scale rotating stall cell has the same flow structure as the flow model.

Moreover, Mailach[10] [11] [12], Marz[13] [14], Hoying[15], and Hah[16] reported that "Rotating Instability" could occur in the compressors with relatively large tip clearance. Rotating instability was a circumferential propagating phenomenon that the leakage vortex inclining at circumferential direction went over or interact the leading edge of the next blade and cause new leading edge separation.

Many researches had been done for the rotating stall or the rotating instability in axial compressor for a long time, and the classification of the form of the phenomenon had been advanced comparing to the centrifugal compressor.

For the centrifugal compressor, Lenneman and Howard[17] experimentally investigated its number and the rotating speed of the rotating stall cells as a typical research on the rotating stall in impeller. And the number of stall cells had tendency to increase depending on the impeller blade number.

Compressor impellers with small blade number and high blade height are often used for automotive turbocharger because of the demand of reduction in size and weight so the aspect ratio has to be small. Tomita[18] investigated an example by experimental and numerical approach that propagating phenomena like the rotating stall or the rotating instability showed unstable behavior in such centrifugal compressor having small blade number. And it was also shown that impellers which induced tip leakage vortex breakdown at high flow rate might stabilize their internal flow structure by generating circumferential uniform blockage region near blade tip at low flow rate.

In this study, authors investigated whether modifying a given impeller to induce the tip leakage vortex breakdown could reduce the surging flow rate or not, and confirmed it experimentally and numerically.

TEST COMPRESSORS

Table 1 shows specifications of the conventional centrifugal compressor for automotive turbocharger. They have open type and back swept impeller. The conventional impeller has 6 full blades

Presented at International Gas Turbine Congress 2019 Tokyo, November 17-22, Tokyo, Japan
Review Completed on March 19, 2020

and 6 splitter blades. The new compressor, which is described later part of this paper, has same blade number and exactly same meridional geometry of the conventional compressor.

Table 1 Specification of the Test Compressors

	Conventional Compressor and New Compressor
Number of full blade	6
Number of splitter blade	6
Impeller inlet diameter	40.1mm
Impeller outlet diameter	51.0mm

NUMERICAL SCHEME

Figure 1 shows computational grid including impeller, diffuser and scroll for this research. The number of grid is about 2,470,000 for the impeller as structured mesh, 410,000 for the diffuser and 250,000 for the scroll as unstructured mesh. Steady and Unsteady CFD were conducted with CFX ver.12 and k-ε turbulence model was applied. 178,000rpm was chosen as the research speed because the conventional compressor has an apparent pressure peak point and surging flow rate increases at that speed comparing to lower speeds.

Frozen-rotor was applied to the boundary condition between rotating part and stationary part in the case of steady CFD. In the unsteady CFD, time step per iteration was 0.0028ms, which corresponded to 20 steps per 1 full blade passing (BPF: Blade Passing Frequency).

Vortex core identification and normalized helicity Hn were applied to visualize internal flow structure. The normalized helicity corresponds to cosine value of angle between vectors of absolute vorticity and relative flow velocity and it is useful to detect vortex breakdown. Hn=+1 represents a clockwise longitudinal vortex, and Hn=-1 represents counterclockwise longitudinal vortex.

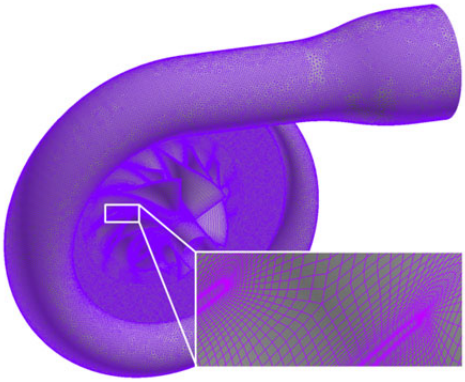

Figure 1 Computational Grid

EXPERIMENTAL SETUP

Installation position of pressure sensors is shown in figure 2. Two sensors were installed at circumferential interval of 30 degree and 3 mm upstream from the blade leading edge. When the scroll end section is determined as a reference position as 0 degree, its tongue is located at approximately 60 degree and the pressure measurement positions are at 90 degree and 120 degree. The sensors will be referred to as sensor 1 and sensor 2 from upstream side in the rotational direction. Two ENDEVCO 8510C-100 sensors were used and their sampling frequency was 500kHz, which corresponds to 28 points per 1 full blade pitch at 178,000rpm.

Pressure waves at impeller inlet were measured to capture unstable disturbance which might be caused by impeller stall near peak pressure point at 178,000rpm. At design point, blade normally makes pressure difference between pressure surface and suction surface by its loading. However, when the impeller stalls, low pressure region of the suction surface at leading edge weakens and the pressure difference between the pressure surface and the suction surface becomes smaller. Although it is preferable to perform the pressure measurement slightly downstream of the leading edge in order to detect the impeller stall, pressure was measured at 3mm upstream of the blade leading edge to avoid interaction with the scroll.

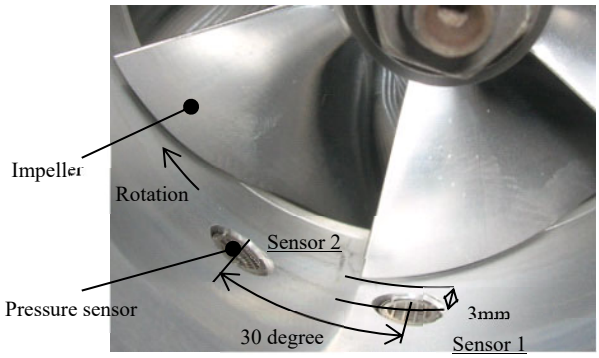

Figure 2 Position of Pressure Sensors

CONVENTIONAL COMPRESSOR

(1) Compressor performance

Figure 3 shows the performance map of the conventional compressor obtained by measurement. The flow ratio Q* as the horizontal axis is normalized by the choking flow rate of the conventional compressor at 178,000rpm, which has a peak pressure point at Q*=0.72 and positive slope. Its operating range becomes narrow at over π=2.4 because its surging flow rate sharply increases at 178,000rpm comparing to lower speeds. The conventional compressor has a typical performance characteristic of centrifugal compressors for automotive turbocharger. The efficiency is also normalized by the maximum efficiency of the conventional compressor.

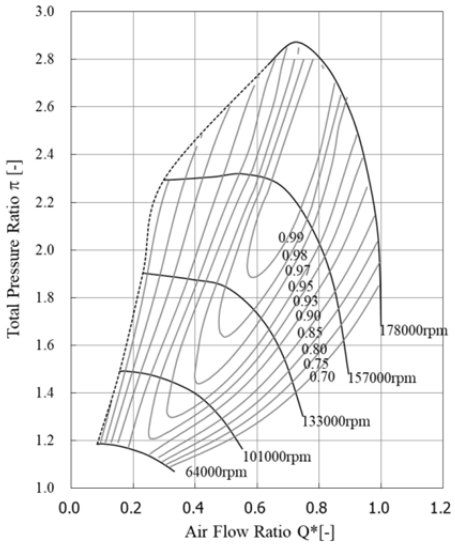

Figure 3 Performance Map of the Conventional Compressor (Measurement)

(2) Pressure Fluctuation Measurement

The pressure waves at the impeller inlet and their FFT analysis results at 178,000rpm are shown in figure 4. Cyclic pressure fluctuation due to the blade passing could be seen at the peak efficiency point (Q*=0.83), and phase difference between the two sensors was 30 degrees. Rotating speed was 2,967Hz and the BPF

of the full blade was confirmed at 17,800Hz. It can be said that the blades work correctly and no unstable fluctuation occur. At peak pressure point (Q*=0.72), BPF amplitude was larger than it at the peak efficiency point. Although BPF component was still dominant, shape of the pressure wave and amplitude were slightly fluctuating. This fact may explain that impeller stall or tip leakage flow fluctuation occurs at this condition. Near the surging point (Q*=0.65), the cyclic BPF disappeared and broad band frequencies appeared. It is thought that unstable rotating stall or rotating instability occurs.

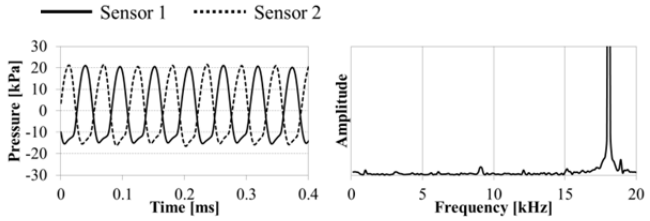

Pressure Fluctuation FFT

(a) Peak Efficiency Point (Q*=0.83)

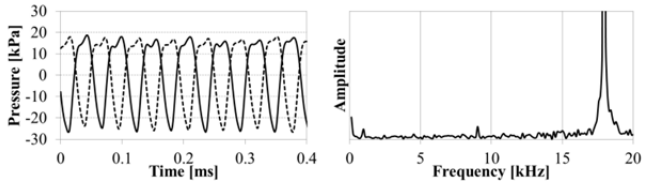

Pressure Fluctuation FFT

(b) Peak Pressure Point (Q*=0.72)

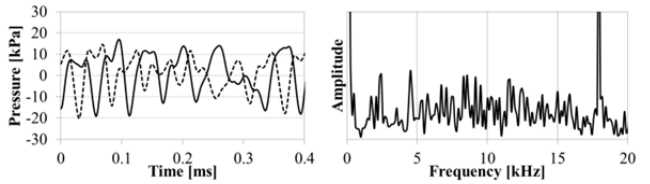

Pressure Fluctuation FFT

(c) Near Surging Point (Q*=0.65)

Figure 4 Pressure Fluctuation at Impeller Inlet (Conventional Compressor, Measurement)

(3) Steady CFD Results

Conventional compressor performance obtained by steady CFD is shown in figure 5. The steady CFD was conducted at choking condition, Q*=0.95 to confirm the performance characteristic, Q*=0.84 as the peak efficiency point, Q*=0.72 as the peak pressure point and Q*=0.60 as well developed stall condition at 178,000rpm. It showed reasonable choke flow rate, efficiency and pressure ratio comparing to the measurement result. Since CFD showed that Q*=0.72 is higher than Q*=0.84 at pressure ratio, the impeller might stall at higher flow ratio in the CFD.

Relative Mach number distribution at the 90% span is shown in figure 6. At Q*=0.84 as a typical peak efficiency point, all of the blades had almost uniform loading and low velocity region due to leakage flow were found. It is naturally thought that no unstable phenomenon has occurred. At Q*=0.72 at the steady CFD, although two of the blades were working normally without low velocity region, a stalled region with large low velocity region was identified. The stall region expanded to half of the impeller at Q*=0.60 and was one large scale stall cell occupying approximately 180 degree.

Mach number distribution near blade tip and identified vortex core colored by normalized helicity in one of the blades at Q*=0.84 is shown in figure 7. The compressor in the figure was rotating clockwise as viewed from the upstream, and the longitudinal tip leakage vortex rolls counterclockwise. Once the tip leakage vortex breakdown occurs, reverse flow generated by adverse pressure gradient makes longitudinal vortex rolling clockwise. If the vortex core shape cannot be maintained, spiral type vortex breakdown occurs. It is found that the tip leakage vortex was not broken in spite of the interaction with shock wave generated near blade suction side in the conventional compressor.

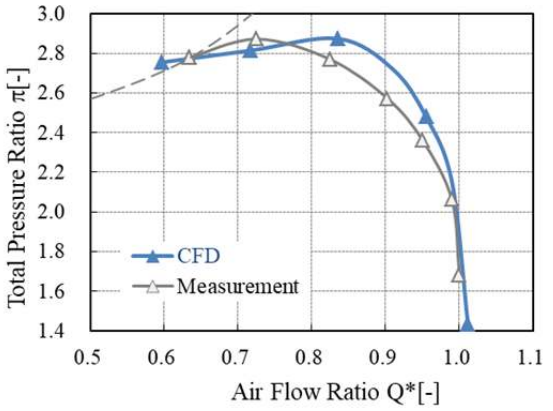

(a) Total Pressure Ratio

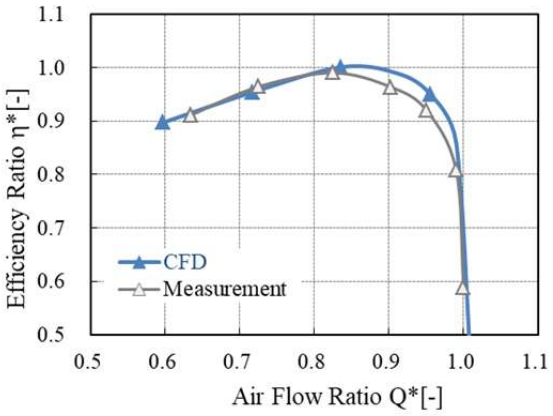

(b) Efficiency Ratio

Figure 5 Performance of the Conventional Compressor at 178,000rpm

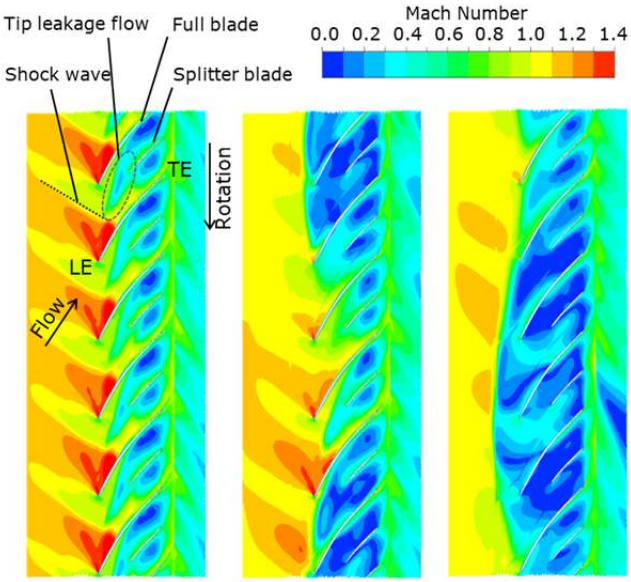

Q*=0.84 Q*=0.72 Q*=0.60

Figure 6 Relative Mach number Distribution at 90% Span (Conventional Compressor, Steady CFD)

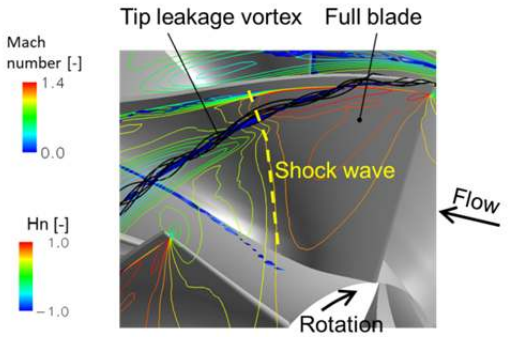

Figure 7 Internal Flow Structure in the Conventional Compressor at Peak Efficiency Point (Q*=0.84, Steady CFD)

(4) Unsteady CFD Results

Unsteady CFD was conducted to research unsteady flow behavior at Q*=0.84, 0.72 and 0.60. Following figures show one rotation or instantaneous result after three rotation calculation. Pressure fluctuation at 3 mm upstream of the impeller leading edge corresponding to the sensor 1 is shown in figure 8. Similar to the measurement, stable cyclic fluctuation can be found at Q*=0.84. At Q*=0.72, although the BPF is still dominant, the shape and amplitude were fluctuating like the measurement result. At Q*=0.60, low frequency phenomenon occurred and the cyclic fluctuation couldn't be seen any more.

Figure 9 shows limiting streamline on suction surface, vortex cores colored by normalized helicity and regions of an axial flow velocity V_z=0m/s in an axial cross section of the impeller leading edge at an instantaneous flow field. From the limiting streamline, it is possible to visualize secondary flow caused by separation on the suction surface or blockage and to easily detect changes in the flow structure. When the tip leakage vortex collapsed or hit next blade, the meridional velocity decreases. At Q*=0.84, the tip leakage vortex were generated but no reverse flow could be found. On the other hand, reverse flow near the blade tip was generated at the half of the blades at Q*=0.72. And tip leakage vortex with positive normalized helicity could be seen there. The reverse regions consisted of the broken tip leakage vortex and reverse flow coming from the secondary flow on the suction surface. The other half of the blades worked normally as Q*=0.84 without reverse flow. The reverse flow region expanded near the surging point at Q*=0.60. And the reverse flow kept its non-uniformity, where the blade 1 stalled but the blade 4 worked normally shown in the figure.

Vortex cores colored by normalized helicity and limiting streamline of the blade 1 and 4 of the figure 9(c) are shown in figure 10. The tip leakage vortex breakdown occurred at the blade 1, and strong secondary flow existed around the blade1. On the other hand, it was found that the blade 4 worked normally with weak secondary flow. Although this kind of vortex structure appeared when a rotating stall occurred, its behavior was strongly unstable like a compressor shown by Tomita[18].

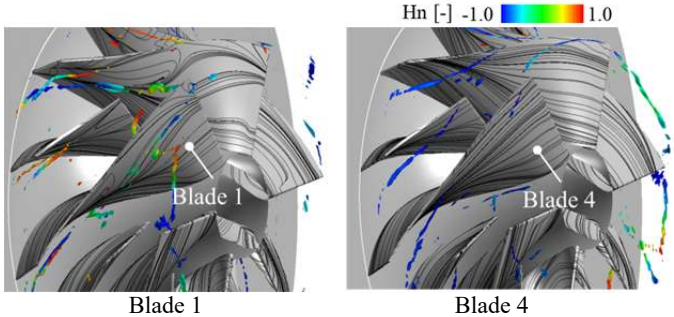

Blade 1 Blade 4

Figure 10 Vortex Cores and Limiting Streamline on Suction Surface near Surging Point (Q*=0.60, Conventional Compressor)

NEW COMPRESSOR

(1) Impeller Design

As shown in the previous chapter, it was found that a circumferential non-uniform blockage region was generated by tip leakage vortex breakdown or stall cells in the conventional impeller. In our past research, it was suggested that impellers which induced tip leakage vortex breakdown at relatively high flow rate might stabilize internal flow by generating circumferential uniform blockage region near blade tip at low flow rate. In this study, authors investigated whether modifying a given impeller to induce the tip leakage vortex breakdown can reduce the surging flow rate or not.

Authors designed a new impeller which had higher loading at

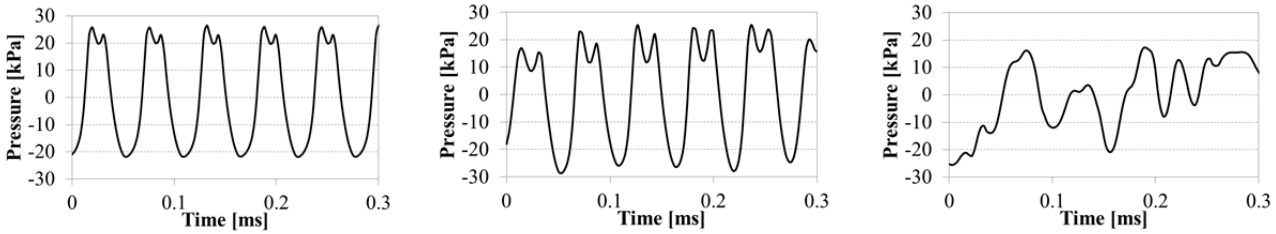

(a) Peak Efficiency Point (Q*=0.84) (b) Peak Pressure Point (Q*=0.72) (c) Near Surging Point (Q*=0.60)

Figure 8 Pressure Fluctuation at Impeller Inlet (Conventional Compressor, Unsteady CFD)

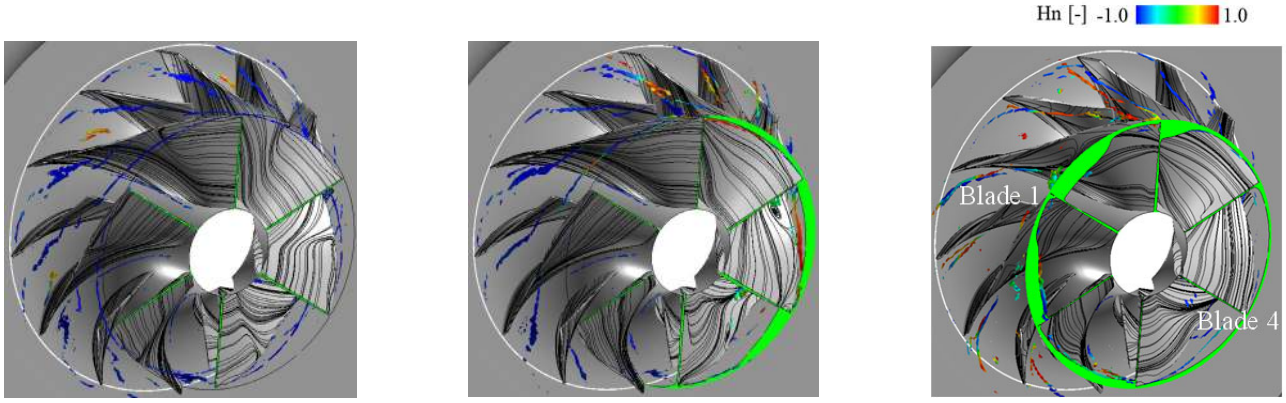

(a) Peak Efficiency Point (Q*=0.84) (b) Peak Pressure Point (Q*=0.72) (c) Near Surging Point (Q*=0.60)

Figure 9 Instantaneous Internal Flow Structure (Conventional Compressor, Unsteady CFD)

the inducer part to strengthen the leakage flow and the secondary flow to generate a circumferential uniform blockage to stabilize the flow field. As shown in Table 1, the main specification such as the number of blades and the meridional geometry such as the blade inlet diameter, the outlet diameter, the blade height were maintained. And the impeller was also designed to increase not only near the inducer loading but also overall loading. Same vaneless diffuser and scroll were used for the new compressor as well.

(2) Numerical Results

Figure 11 shows steady CFD result at the peak efficiency point (Q*=0.84) at 178,000rpm. Bubble type tip leakage vortex breakdown interacted with shock wave could be seen at all of the blades.

Unsteady CFD was performed on the newly designed compressor as well as the conventional one. Figure 12 shows pressure fluctuation at 3 mm upstream of the impeller leading edge as the conventional compressor. Stable cyclic BPF can be clearly found at Q*=0.84 and it is same as the conventional compressor. Unsteady phenomena was not detected in the new compressor at least at Q*=0.72 in spite of the fact that unstable phenomena happened in the conventional compressor. At Q*=0.60, low frequency disturbance occurred and the cyclic fluctuation couldn't be seen as well as the conventional compressor.

Same as figure 9, figure 13 shows limiting streamline on suction surface, vortex cores colored by normalized helicity and regions of an axial flow velocity V_z=0m/s in an axial cross section of the impeller leading edge at an instantaneous flow field. No reverse flow appeared at Q*=0.84. Reverse flow caused by the tip leakage vortex breakdown and secondary flow near the blade tip could be found at all of the blades at Q*=0.72 but their scale and condition of the limiting streamline were almost uniform. Although the reverse flow region expanded at Q*=0.60.

(3) Performance

Figure 14 shows the pressure ratio and the efficiency ratio obtained by a performance test. As a result of the performance test of the new impeller, considering that the surging flow rate at the same shaft speed is reduced by 3% and the pressure ratio at the surging point has been improved from 2.8 to 2.9, the surging flow rate at the pressure ratio of 2.8 can be reduced by 8%. In this way, although efficiency ratio was deteriorated by 0.03pt, it was found that the tip leakage flow was dominant with the stall phenomenon of the centrifugal compressor.

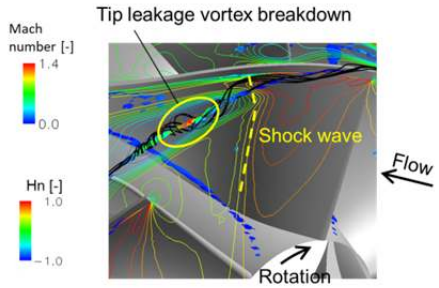

Figure 11 Internal Flow Structure in the New Compressor at Peak Efficiency Point (Q*=0.84, Steady CFD)

CONCLUSION

In this study, authors investigated whether modifying a given impeller to induce the tip leakage vortex breakdown can reduce the surging flow rate or not.

Unsteady CFD revealed that circumferential uniform blockage region generated by weak tip leakage vortex breakdown was seen in the new compressor, which increased its inducer loading, and the blockage region gradually developed from the peak efficiency condition to near surging condition. It is thought that the uniform blockage region can keep the internal flow stable in the new compressor, in spite of the fact that non-uniform complex phenomena happened in the conventional compressor.

As a result of the performance test of the new impeller, the surging flow rate at the pressure ratio of 2.8 can be reduced by 8%. In this way, it was found that the tip leakage flow is dominant with the stall phenomenon of the centrifugal compressor, and it is confirmed that the tip leakage vortex control is one of the effective

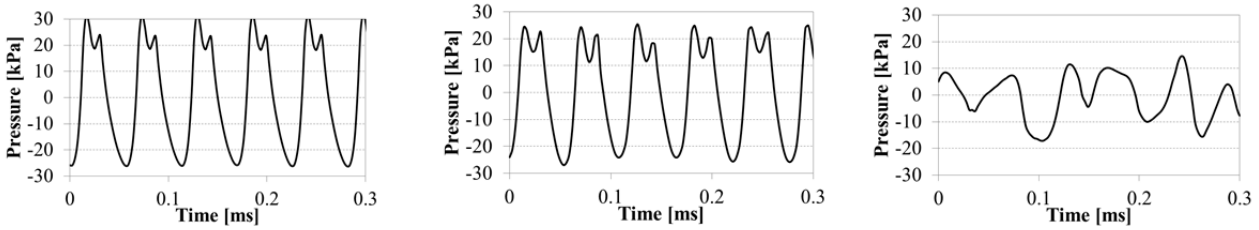

(a) Peak Efficiency Point (Q*=0.84) (b) Peak Pressure Point (Q*=0.72) (c) Near Surging Point (Q*=0.60)

Figure 12 Pressure Fluctuations at Impeller Inlet (New Compressor, Unsteady CFD)

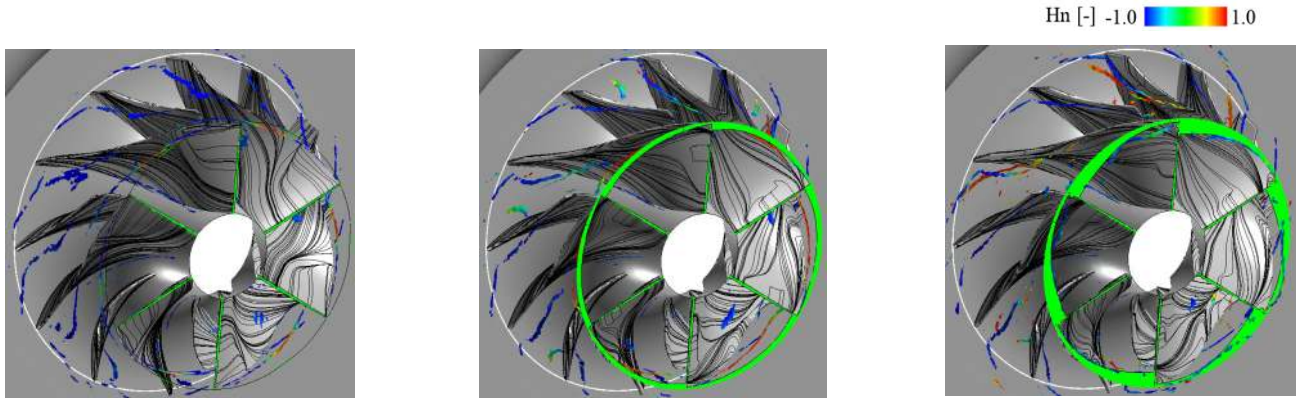

(a) Peak Efficiency Point (Q*=0.84) (b) Peak Pressure Point (Q*=0.72) (c) Near Surging Point (Q*=0.60)

Figure 13 Instantaneous Internal Flow Structure (New Compressor, Unsteady CFD)

means for the operation range enhancement. Since authors have not done any optimization on the loading design, research to find the best tuning to minimize the efficiency loss can be done with CFD as a future work.

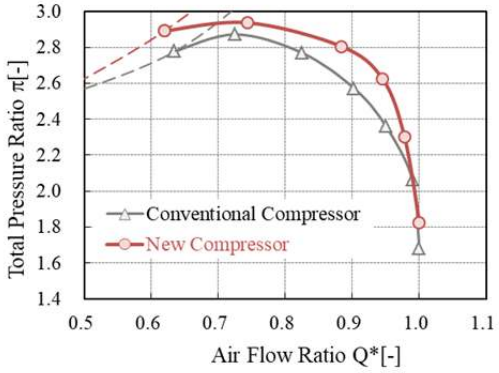

(a) Total Pressure Ratio

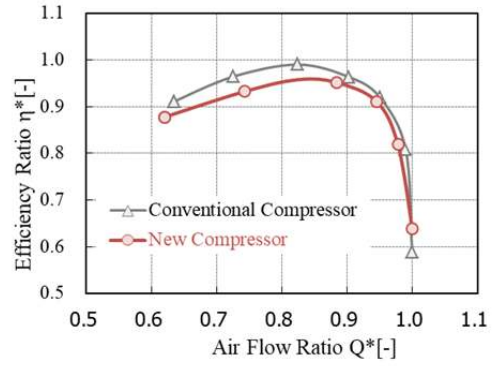

(b) Efficiency Ratio

Figure 14 Performance Comparison at 178,000rpm (Measurement)

REFERENCES

[1] Moore, F. K., and Greitzer, E. M., 1986, "A Theory of Post-Stall Transient in Axial Compression Systems: Part1 Development of Equations," Trans. ASME, Journal of Engineering for Gas Turbines and Power, Vol.108, pp.69-76.

[2] Moore, F. K., and Greitzer, E. M., 1986, "A Theory of Post-Stall Transient in Axial Compression Systems: Part2 Application," Trans. ASME, Journal of Engineering for Gas Turbines and Power, Vol.108, pp.231-239.

[3] McDougall, N. M., Cumpsty, N. A., and Hynes, T. P., 1990, "Stall Inception in Axial Compressors," Trans. ASME, Journal of Turbomachinery, Vol.112, pp.116-125.

[4] Garnier, V. H., Epstein, A. H., and Greitzer, E. M., 1991, "Rotating Waves as a Stall Inception Indication in Axial Compressors," Trans. ASME, Journal of Turbomachinery, Vol.113, pp.290-301.

[5] Day, I. J., 1993, "Stall Inception in Axial Flow Compressors," Trans. ASME, Journal of Turbomachinery, Vol.115, pp.1-9.

[6] Poensgen, C. A., and Gallus, H. E., 1996, "Rotating Stall in a Single-Stage Axial Flow Compressor," Trans. ASME, Journal of Turbomachinery, Vol.118, No.2, pp.189-196.

[7] Inoue, M., Kuroumaru, M., Tanino, T., and Furukawa, M., 2000, "Propagation of Multiple Short Length-Scale Stall Cells in an Axial Compressor Rotor," Trans. ASME, Journal of Turbomachinery, Vol.122, pp.45-54.

[8] Inoue, M., Kuroumaru, M., Tanino, T., Yoshida, S., and Furukawa, M., 2001, "Comparative Studies on Short and Long Length-Scale Stall Cell Propagating in an Axial Compressor Rotor," Trans. ASME, Journal of Turbomachinery, Vol.123, No.1, pp.24-32.

[9] Yamada, K., Furukawa, M., and Inoue, M., 2002, "Numerical Analysis of Rotating Stall Inception in an Axial Compressor Rotor," Proceedings of the 5th JSME-KSME Fluids Engineering Conference.

[10] Mailach, R., 1999, "Experimental Investigation of Rotating Instabilities in a Low-Speed Research Compressor," I. Mech. E, C557/006, pp.595-604.

[11] Mailach, R., Sauer, H., and Vogeler, K., 2001, "The Periodical Interaction of The Tip Clearance Flow in The Blade Rows of Axial Compressors," ASME Paper, 2001-GT-0299.

[12] Mailach, R., Lehmann, I., and Vogeler, K., 2001, "Rotating Instabilities in an Axial Compressor Originating from the Fluctuating Blade Tip Vortex," Trans. ASME, Journal of Turbomachinery, Vol.123, pp.453-463.

[13] Marz, J., Gui, X., and Neise, W., 1999, "On the Structure of Rotating Instabilities in Axial Flow Machines," 14th ISABE Paper, No.99-7252.

[14] Marz, J., Hah, C., and Neise, W., 2002, "An Experimental and Numerical Investigation into the Mechanisms of Rotating Instability," Trans. ASME, Journal of Turbomachinery, Vol.124, pp.367-375.

[15] Hoying, D., Tan, C. S., Huu Doc Vo, and Greitzer, E. M., 1999, "Role of Blade Passage Flow Structures in Axial Compressor Rotating Stall Inception," Trans. ASME, Journal of Turbomachinery, Vol.121, No.2, pp.735-742.

[16] Hah, C., Schulze, R., Wagner, S., and Hennecke, D. K., 1999, "Numerical and Experimental Study for Short Wavelength Stall Inception in a Low-Speed Axial Compressor," 14th ISABE, No.99-7033.

[17] Lenneman, E. and Howard, J. H. G., 1970, "Unsteady Flow Phenomena in Rotating Centrifugal Impeller Passages," Trans. ASME, Journal of Engineering for Power, Vol.92, No.2, pp.65-72.

[18] Tomita, I., Ibaraki, S., Furukawa, M., and Yamada, K., 2013, "The Effect of Tip Leakage Vortex for Operating Range Enhancement of Centrifugal Compressor," ASME, Journal of Turbomachinery, Vol.135, No.5, 051020-1-8